Grid Side Converter Controller Optimized for DFIG Driven Wind Turbine Based on Type-2 Fuzzy Logic

Ossama E. Gouda, Ebtisam M. Saied, Omar. M. Salim, Mohamed I. Awaad

Abstract— Grid side system GSS model is studied and developed in steady state form by using phasor theory; studying the relationships between active and reactive powers, voltage, and currents at different operating modes. Then, control of the grid side converter GSC is optimized; developing the grid side dynamic model based on space vector theory. In this paper vector control technique that utilizes a rotating reference frame (dq) aligned to the grid voltage space vector is employed. This control algorithm made it possible to achieve the two main objectives of GSC: control of the DC bus voltage and assure transmission of power through the converter (along with controlled reactive power exchange). DC link bus voltage has been controlled using Interval Type-2 Fuzzy Logic Controllers (IT2FLCs). The proposed IT2FLCs were designed to deal with the ambiguity appeard as a result of changes during system operation. In this paper, design of GSC controller, which is responsible for the terminal voltage control in addition to the DC link voltage regulation, is performed. The developed IT2FLC controller is simulated using MATLAB/SIMULINK software for a 1.5 MW typical wind turbine to verify the performance of the controller.

Index Terms— Doubly Fed Induction Generator, Grid Side Converter control, Interval Type-2 Fuzzy Controllers, Wind power generation.

1 Introduction

WIND power has become the most significant option among renewable energy source based electricity generation due to its wider availability and very low environmental pollution [1]. Data published annually by the Global Wind Energy Council (GWEC) show that global annual wind capacity additions increased from 15.2 GW in 2006 to 41.2 GW in 2011, i.e. at an average annual rate of growth of 22%. Growth slowed to less than 9% in 2012, with 44.8 GW of new capacity added (GWEC, 2013) and contracted by more than 20% in 2013, when 35.5 GW was added (global cumulative capacity reached 318.1 GW by the end of 2013 (GWEC, 2014) [2]. However, stability and power quality problems exist due to the intermittent nature of the wind. This problem becomes evident, especially, when the amount of wind power integrated to the system is significantly large. The output voltage variations of a wind farm occur due to two major reasons: (i) the wind gusts and frequent gradual wind speed variations and (ii) mechanical disturbances such as swings in the wind turbine, wind shear effect and tower shadow effect. Wind power plants are vulnerable during certain transient states. For instance, they are susceptible for tripping during system short circuit fault, due to their low inertia constant [3].The wide spread use of wind generation on power network demands that the wind farms should be able to contribute to network support as the conventional synchronous generators do. Hence, new grid codes are emerging which lay down the requirements that should be fulfilled by the wind power developers [4]. These grid codes mainly consider the performance of the wind farm with respect to voltage control capability, reactive exchangeable range capability, frequency control ability and fault ride through capability.

DFIG is a wound rotor induction motor with rotor injection. The speed of the DFIG can be controlled by injecting a variable voltage of slip frequency to the rotor. It has become popular in wind farms, since it enables maximum energy extraction due to its variable speed operation capability [1], [5]. In this paper; control of the GSC is tested by studying steady state and dynamic models of the GSS formed by the grid, the grid side filter, and GSC itself. Moreover, the vector control strategy for GSC is studied. This control strategy enables to fulfil the two main objectives of GSC which are: control the DC link terminal voltage of and control of active and reactive powers exchanged directionally between the machine rotor and the grid.

2 Steady State Model of GSS

The system configured by GSC, filter, and grid voltage can ideally be represented as shown in Fig. 1. The grid voltage (vag, vbg, vcg) are sinusoidal with constant amplitude and frequency. The voltage imposed by GSC (v_{af}, v_{bf}, v_{cf}) can be modified in both amplitude and phase. The filter considered is a simple filter with a pure inductive part (L_f) and a parasitic resistance (R_f).

For analysis purposes, if an ideal GSS is considered, its equiva lent to a single-phase GSS as illustrated in Fig. 2. Thus, it is only necessary to analyze one phase then extrapolate to the other two phases. The output voltage generated by the converter depends on the characteristics of the converter itself (two-level, multilevel topology, etc.) and the modulation technique employed. Under steady state operating conditions, all system magnitudes (v_{af}, i_{ag}, v_{ag}) have constant amplitude, fre-

- *M. I. Awaad is currently working as a teaching assistant and pursuing doctoral degree program in electrical power and machines at Benha University, Egypt. E-mail: Mohamed.awad@bhit.bu.edu.eg*
- *Omar. M. Salim is currently an assistant professor in electrical power and machines Department, Benha Faculty of engineering, Benha University, Egypt. E-mail: omar.salim@bhit.bu.edu.eg*

quency and phase shift between each and other corresponding component in their three phase system [5].

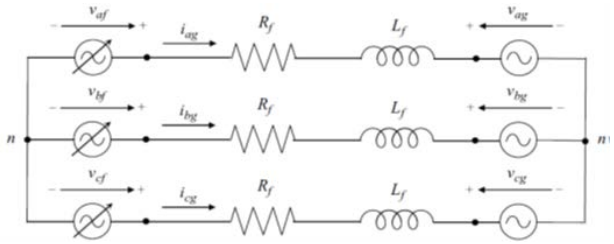

Fig. 1. A simplified representation of the three-phase grid system.

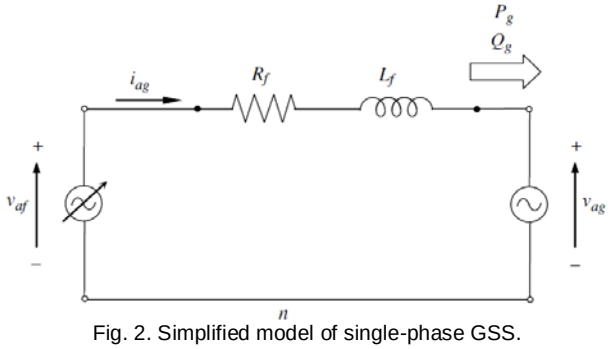

Fig. 2. Simplified model of single-phase GSS.

The maximum achievable fundamental output voltage by the converter (in linear modulation, by SVM or by sinusoidal PWM with third harmonic injection) depends on the DC bus voltage:

$$v_{af} = \frac{v_{bus}}{\sqrt{3}} \quad (1)$$

Thus, the voltage imposed by the converter can be modified depending on the requirements of the application. So under steady state operation, the electrical equation of the system represented in Fig. 2 is:

$$V_{af} = V_{ag} + (R_f + jL_f w_s) I_{ag} \quad (2)$$

Where; V_{af}, V_{ag}, and I_{ag} phasor representation used for the steady state. The general phasor diagram is shown in Fig. 3, which has been built based on the following steps:

- First, the grid voltage phasor is drawn with a phase angle that can be arbitrarily chosen (Fig. 3a).
- Second, grid current is drawn knowing the phase shift between the grid voltage and current (Fig.3b).
- Third, once the current is drawn, the voltage drop in the filter can be calculated and accordingly drawn (Fig. 3c).
- Fourth, the voltage of the converter is calculated and drawn (Fig. 3d), while Vaf is considered to be the phasor representation of the fundamental voltage of the converter output voltage.

The power flow study is normally carried out in the grid voltage (V_{ag}) rather than in the converter (V_{af}). Hence, the active and reactive powers are calculated in the grid voltage point (single phase).

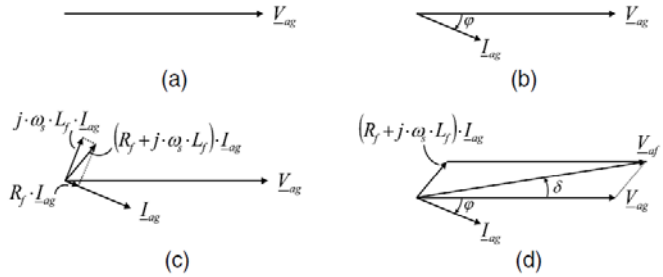

Fig. 3. Phasor diagram construction of GSS.

$$P_g = |V_{ag}| . |I_{ag}| . \cos\varphi \quad (3)$$

$$Q_g = |V_{ag}| . |I_{ag}| . \sin\varphi \quad (4)$$

The power sign convention adopted in this paper is shown in Fig. 4. When $P_g>0$, the converter is delivering power to the grid; whereas when $P_g<0$, the converter is receiving power from the grid.

Two particular operating conditions exist for GSC while transmitting active power in both directions (positive and negative), but with unity power factor, that is, zero reactive power exchange at the grid point. Fig. 5 shows these two particular cases, where the current is zero shifted (grid receiving power from the converter) or 180 (grid delivering power to the converter) [5].

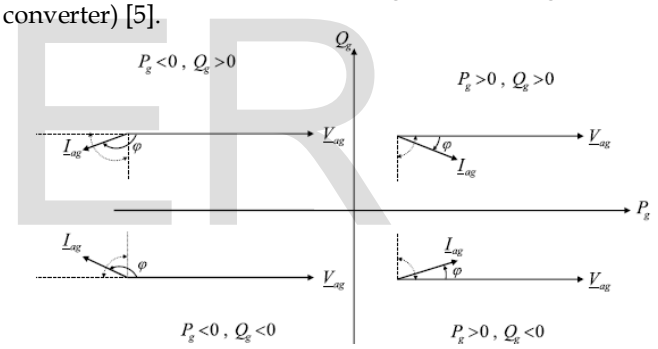

Fig. 4. Power sign convention

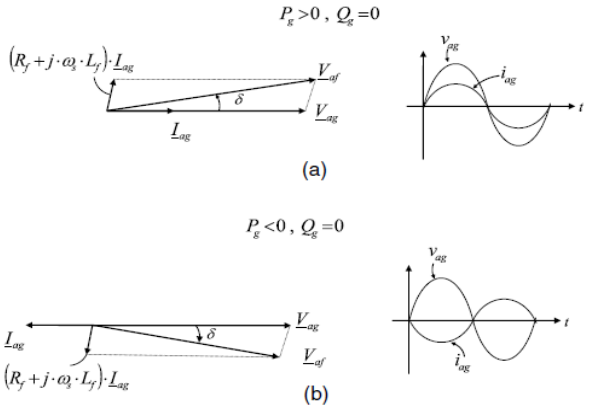

Fig. 5. Phasor diagrams at unity power factor: (a) $P_g>0$ and (b) $P_g<0$.

$$P_g = \frac{|V_{ag}| \cdot |V_{af}|}{w_s L_f} \sin\delta \, with \, R_f \to 0 \quad (5)$$

$$P_g = |V_{ag}| \frac{|V_{af}| \cos\delta - |V_{ag}|}{w_s L_f} with \, R_f \to 0 \quad (6)$$

Therefore, it is possible to know the active and reactive power flow through the grid, if only the converter voltage amplitude and phase shift with respect to the grid voltage is known.

3 Vector Control of GSS

Control is a necessary part of GSS; without having control of some of the magnitudes of the grid side part, it is not possible to make it work properly. Vector control based schema is studied. This control technique is widely extended among the control strategies for grid connected converters. It provides good performance characteristics with reasonably simple implementation requirements. The vector control technique follows the philosophy of representing the system that is going to be controlled in our case; GSS in a space vector form.

3.1 Grid Voltage Oriented Vector Control of GSC

The grid voltage oriented vector control (GVOVC) is the controlling part of the power flow of the DFIG. The power generated by the wind turbine is partially delivered though the rotor of the DFIG. This power flow that goes through the rotor flows also through the DC link and finally is transmitted by GSC to the grid. The simplified block diagram of GSS, together with a schematic of its control block diagram, are given in Fig. 6. Subsequent paragraphs give the basic principles of control of GSC. In this case, for a simpler exposition, the VSC topology chosen to present the control is a 2L-VSC. However, from a vector control point of view, nothing will change if a multilevel VSC topology is used.

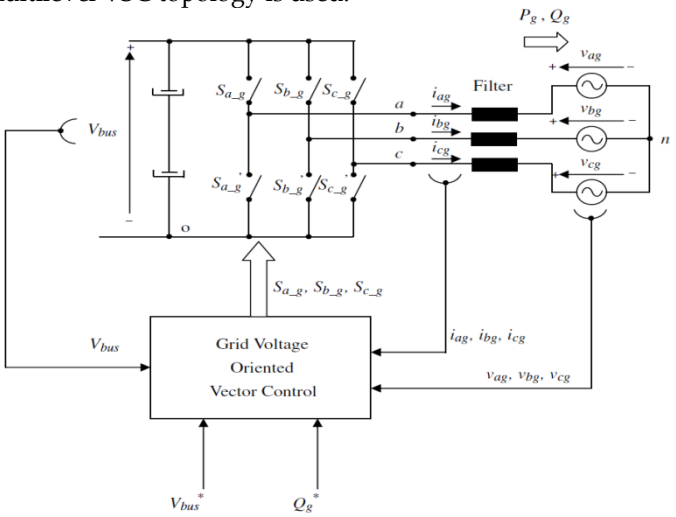

Fig. 6. Grid Side System control [5].

The pulses for the controlled switches (S_{ag}, S_{bg}, S_{cg}) of the 2L-VSC, that is, the output voltage of the converter, are generated in order to control the DC bus voltage (V_{bus}) of the DC link and the reactive power exchanged with the grid (Q_g); generally done according to a closed loop control law. Some typical controls are vector control or direct power control. However, this section only studies the grid voltage oriented vector control.

On the other hand, control of V_{bus} is necessary since, as seen in previous sections, the DC link is mainly formed by a capacitor. Thus, the active power flow through the rotor must cross the DC link and then it must be transmitted to the grid. Therefore, by only controlling the Vbus variable to a constant value, this active power flow through the converters is ensured, together with a guarantee that both grid and rotor side converters have the required DC voltage to work properly.

GVOVC block diagram is shown in Fig. 7. From the Vbus and Q_g references, it creates pulses for the controlled switches S_{ag}, S_{bg}, and S_{cg}. Thus, the modulator creates the pulses S_{ag}, S_{bg}, S_{cg} from the abc voltage references for GSC: v_{af}, v_{bf}, and v_{cf}. These abc voltage references are first created in dq coordinates (v_{df}, v_{af}), then transformed to ab coordinates (v_{af}, v_{bf}), and finally generate the abc voltage references. Then, the dq voltage references (v_{df}, v_{af}) are independently created by the dq current (i_{dg}, i_{qg}) controllers. This indicates that by modifying v_{df}; i_{dg} is mainly modified; while by modifying v_{qf}; i_{qg} is mainly modified. There is also one coupling term in each equation that is best considered in the control as a feed-forward term (at the output of the current controllers), for better performance in the dynamic responses:

$$e_{df} = -w_s L_f i_{qg} \quad (7)$$

$$e_{qf} = -w_s L_f i_{dg} \quad (8)$$

Under ideal conditions, the term v_{dg} is equal to the grid voltage amplitude and is constant as mentioned before. It must be highlighted that the current references (i_{dg}, i_{qg}) are totally decoupled from the active and reactive powers, thanks to the alignment of the grid voltage space vector and the d axis of the rotating reference frame. Thus, i_dg control implies P_g control, while i_qg control implies Q_g control.

$$K_{Pg} = \frac{1}{1.5 v_{dg}} \quad (9)$$

$$K_{Qg} = \frac{1}{-1.5 v_{dg}} \quad (10)$$

As mentioned before, the power P_g reference is created by the V_{bus} regulator.

Indirectly, by this loop, active power flow through the back-to-back converter is ensured.

Finally, for voltage and current coordinate transformations, the angle of the grid voltage is needed. In general, this angle is estimated by a phase locked loop (PLL).

Its closed loop nature provides stability and perturbation rejections to the angle estimation. Consequently, the presented control strategy is able to control the variables (V_{bus}, Q_g) as specified, providing also good dynamic response performance due to its vector control structure.

4 Reactive Power Characteristic of A DFIG

WIND TURBINE

4.1 Power Relationship of a DFIG Wind Turbine

The topology of a DFIG is shown in Fig. 8. The stator of a DFIG is connected to the power grid directly, while the rotor is connected to the grid through two back-to-back pulse width modulation (PWM) converters, i.e. rotor-side converter (RSC) and GSC. GSC usually works at the unity power factor of 1 and is in charge of maintaining a constant DC-link voltage for RSC.

The decoupling control of active and reactive power of the DFIG is achieved by adjusting the rotor's current and voltage through RSC [6].

In Fig. 8, P_T is the input mechanical power from the wind turbine, P_s and Q_s are the output active and reactive power generated by the DFIG. P_c and Q_c are the active and reactive power to GSC from the DFIG.

P_g and Q_g are the active and reactive power to the grid from the DFIG. P_r and Q_r are the active and reactive power to the rotor winding from RSC.

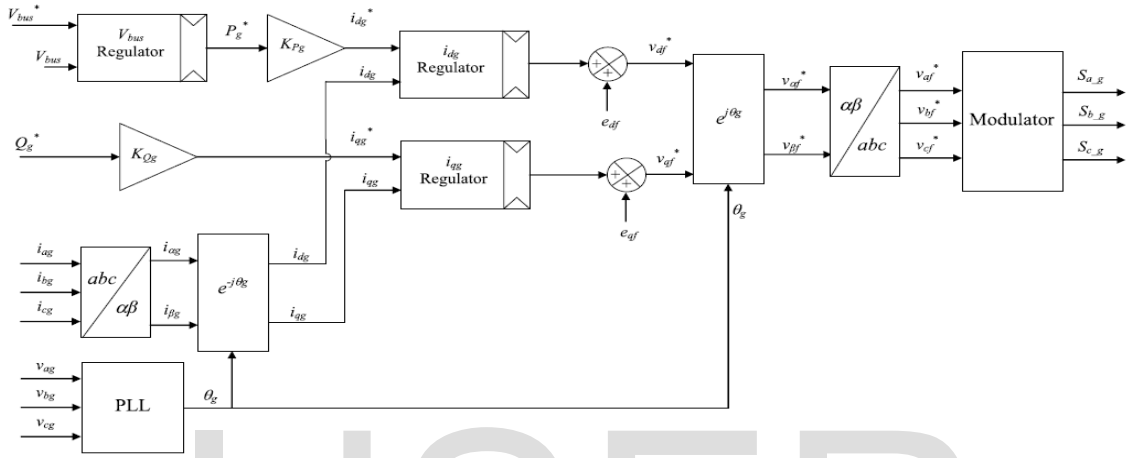

Fig. 7. GVOVC block diagram [5].

Assuming that the input mechanical power is completely converted into the electromagnetic power, the power relationship of DFIG can be presented as:

$$P_T = P_s - P_r \tag{11}$$

The difference between the stator speed and the synchronous speed results in the slip power of the rotor, which is named as the rotor power P_r. Therefore the power relationship can also be expressed as:

$$\begin{cases} P_s = \dfrac{P_T}{(1-s)} \\ P_r = \dfrac{sP_T}{(1-s)} \end{cases} \tag{12}$$

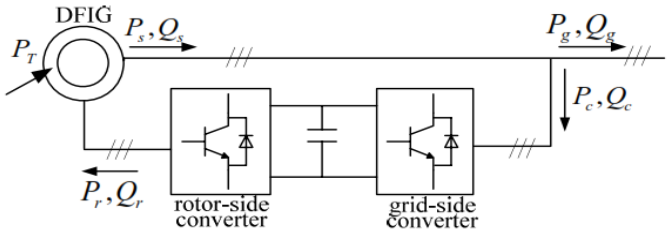

Fig. 8. Topology of a DFIG [5].

4.2 Reactive Power Limitations of GSC

RSC and GSC only transfer active power, while the reactive power Q_c and Q_r are decoupled. If the power loss is neglected, there is $P_c = P_r$.

Since GSC usually works at the unity power factor, that is $Q_c = 0$. However, Q_r is divided into two parts, one part flows into the rotor, and the other part is transferred to the stator by a certain percentage (slip ratio). Therefore, the capacity of RSC is larger than that of GSC. As a result, when analyzing the reactive power limitations of GSC, only the capacity of itself is considered.

For a low wind speed, GSC does not make full use of its capacity. When the grid requires extra reactive power, GSC can be adjusted into a non-unity power factor to meet the requirement. Assuming the maximum capacity of GSC is S_{cmax}, there is

$$P_c^2 + Q_c^2 \le S_{c\,max}^2 \tag{13}$$

The reactive power that GSC can generate or absorb is presented as:

$$-\sqrt{S_{c\,max}^2 - P_c^2} \le Q_c \le \sqrt{S_{c\,max}^2 - P_c^2} \tag{14}$$

Combining (2) and (3), the reactive power limitations of GSC can be illustrated as:

$$Q_{c\,max} = \sqrt{S_{c\,max}^2 - (sP_s)^2} \tag{15}$$

$$Q_{c\,min} = -\sqrt{S_{c\,max}^2 - (sP_s)^2} \tag{16}$$

4.3 Reactive Power Limitations of the DFIG Stator

Based on the orientation of the grid voltage vector, the rotor current can be expressed as [6]:

$$\begin{cases} i_{rd} = \dfrac{L_s}{L_m} i_{sd} \\ i_{rq} = \dfrac{L_s}{L_m} i_{sq} - \dfrac{u_s}{L_m w} \end{cases} \quad (17)$$

where i_{rd} and i_{rq} are the d- and q-axis components of the rotor current, i_{sd} and i_{sq} are the d- and q-axis components of the stator current, L_s is the stator inductance, L_m is the mutual inductance of stator and rotor, u_s is the stator voltage, and ω is the synchronous angular velocity. It is well known that

$$i_{rd}^2 + i_{rq}^2 = i_r^2 \quad (18)$$

So, there is

$$\left(\frac{L_s}{L_m} i_{sd}\right)^2 + \left(\frac{L_s}{L_m} i_{sq} - \frac{u_s}{L_m w}\right)^2 = i_r^2 \le I_{r\,max}^2 \quad (19)$$

where; $I_{r\,max}$ is the maximum current of RSC. Similarly, the stator current can be written as:

$$i_{sd}^2 + i_{sq}^2 = i_s^2 \le I_{s\,max}^2 \quad (20)$$

where; I_{smax} is the maximum current of the stator. The active and reactive power of DFIG stator can be presented as [6]:

$$\begin{cases} P_s = 1.5 u_s i_{sd} \\ Q_s = 1.5 u_s i_{sq} \end{cases} \quad (21)$$

Then,

$$\begin{cases} i_{sd} = \dfrac{2P_s}{3u_s} \\ i_{sq} = \dfrac{2Q_s}{3u_s} \end{cases} \quad (22)$$

According to (22), the reactive power limitations of DFIG stator are shown in Fig. 9, where, the solid line is the boundary values of reactive power.

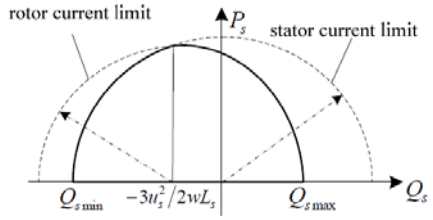

Fig. 9. Reactive power limitations of DFIG stator [6]

5 Interval Type-2 Fuzzy System

Prior to the 20th century; science was considered to be empty from uncertainty. Scientific progress showed that there are many methods which became able to formulate the real world, and overcome uncertainties [7]. Fuzzy logic controllers (FLCs) have been successfully and widely applied to various fields for decades. Basically, FLC is based on human's experience and knowledge resulting that the precise and accurate description of mathematical model of the controlled plant [8].

5.1 Type-2 Fuzzy Set And Membership Function

Type-2 fuzzy logic sets (T2FLSs) were introduced by Zadeh in 1975 [7, 8]. The concept of T2FLS was initially proposed as an extension of classical type-1 fuzzy logic systems (T1FLS) [9]. In Fig. 10, the same input p is applied to the three different types of fuzzy sets, resulting in a degree of membership which is specific to the type of fuzzy set. The amount of uncertainty that is associated is shown in shaded areas, in the same figure, below each type-2 membership function (MF), the secondary MFs (third dimension) is illustrated for each type of fuzzy sets. A T2FLS, denoted $\tilde{A}$, is characterized by a type-2 membership function $\mu\tilde{A}(x,y)$, where $x \in X$, and $u \in [0,1]$, that is,

$$\tilde{A} = \left\{ \left((x,u), \mu_{\tilde{A}}(x,u) \right) | \forall x \in X \ , \forall u \in J_x \subseteq [0,1] \right\} \quad (23)$$

in which $0 \le \mu\tilde{A}(x,y) \le 1$. $\tilde{A}$ can also be expressed as [8, 10];

$$\iint_{x \in X, u \in J_x} \frac{\mu_{\tilde{A}}(x,u)}{(x,u)} J_x \subseteq [0,1] \quad (24)$$

At each value of x, say $x = x_1$, the 2D plane whose axes are u and $\mu_{\tilde{A}}(x_h, u)$ is called a vertical slice of $\mu_{\tilde{A}}(x,u)$. It is $\mu_{\tilde{A}}(x=x_1,u)$ for $x_1 \in X$ and $u \in J_x \subseteq [0,1]$, that is,

$$\mu_{\tilde{A}}(x = x_1, u) = \mu_{\tilde{A}}(x_1) = \int_{u \in J_{x1}} \frac{f_{x1}(u)}{u} J_x \subseteq [0,1] \quad (25)$$

in which $0 \le fx1(u) \le 1$, and $f_{x1}(u)$ is a T1FLS,which is referred to as a secondary set of IT2FLS. When the secondary set is set to unity, i.e. $f_{x1}(u)=1$, an interval type-2 MF, which is a special and simplified form of T2FLS, reflects a uniform uncertainty at the primary memberships of x [8, 10].

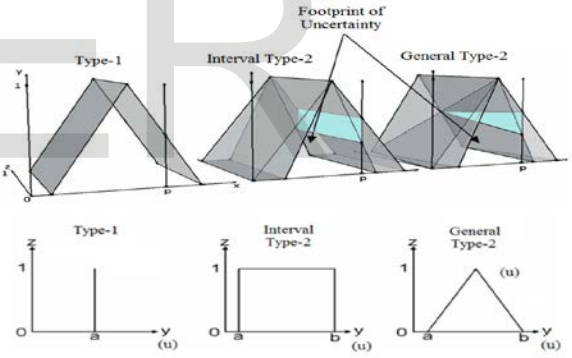

Fig. 10. Three different types of type-2 fuzzy sets with the same input p, the secondary MF introduce the third dimension shown below each [7]

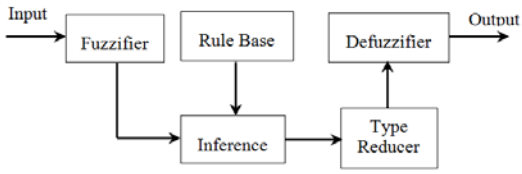

Fig. 11. The IT2FLC block diagram [7,8]

5.2 Structure of a Type-2 Fuzzy Logic System

Very similar to a type-1 fuzzy logic system (TIFLS) structurally, a type-2 fuzzy logic system (T2FLS) also contains the components as: fuzzifier, rule base, fuzzy inference engine, and output processor as shown in Fig. 11 [8]. Unlike T1FLS; T2FLS output processor has an additional part called type reducer represents a mapping of a T2FLS into a T1FLS [8]. Type-reduction in T2FLS is an "extended" version of the defuzzification operation in T1FLS, where the output type-2 MF is reduced to multiple type-1 MFs in order to be defuzzified by the

same T1FLS defuzzifier. Well known types of type reduction are: Centroid, Center-of-Sums, Height, Modified Height and Center-of-Sets (COS) [10].

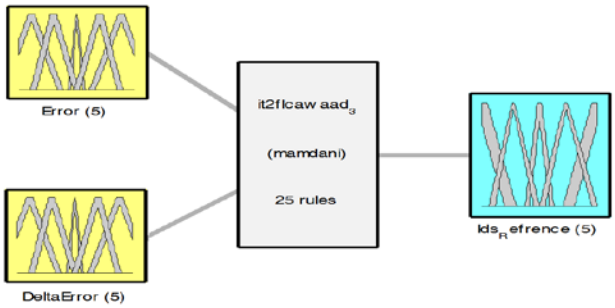

Fig. 12. Block diagram of proposed IT2FLC

6 RESULTS AND DISCUSSIONS

Simulation is carried out on a 1.5 MW turbine. The model is created using MATLAB/SIMULINK. The block diagram presented in Fig. 12 shows the proposed IT2FLC controller structure, Fig. 13 shows an IT2FLC controller rules where in Fig. 14 the simulation of the surface control is presented. The difference between measured and reference DC voltage (Error) and its derivative (ΔE) are chosen as inputs to the IT2FLC and the output is the reference direct current Id*. The proposed controller also uses five linguistic variables. Rules that are presented in Table I have been deduced from [11, 12]. The type-2 Fuzzy logic toolbox used in this paper is customized for Interval type-2 FLS which is a simplified version of general type-2 fuzzy logic system. Center-of-sets type-reduction method is also adopted for this toolbox [13].

Fig. 15 and Fig. 16 represent grid three phase voltage and current in per unit. Grid current references calculated by the outer control loops; are usually given as dq currents components, therefore, to transform the references to αβ frame. Information about the grid voltage phase is obtained using a simple synchronous reference frame PLL [5]. Fig.17 and Fig.18 present the direct and quadrature currents of GSC.

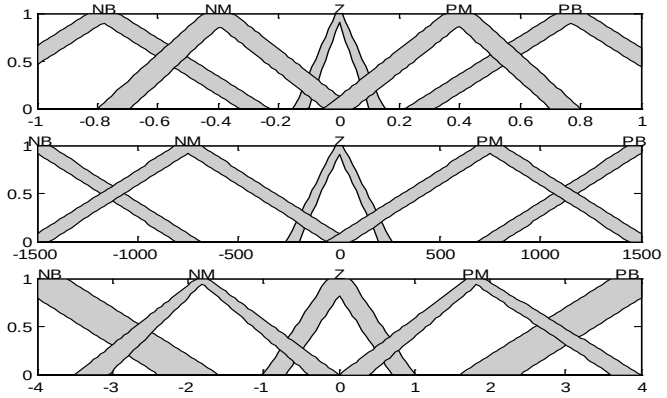

Fig. 13. Membership Functions of proposed IT2FLC

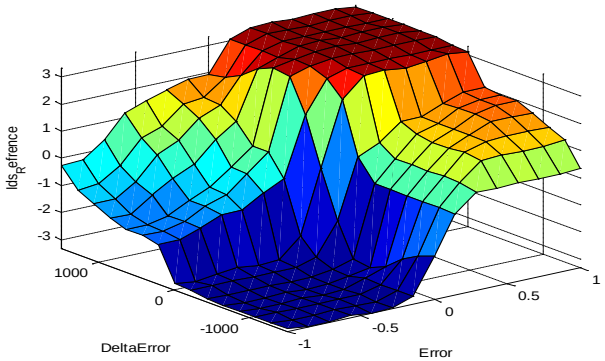

Fig. 14. Surface view of proposed IT2FLC

TABLE I

PROPOSED CONTROL OUTPUT OF IT2FLC

Delta Error \ Error	*NB*	*Z*	*PM*	*NM*	*PM*
NB	NB	NM	Z	NB	Z
Z	NB	Z	PB	NB	PB
PB	Z	PM	PB	PM	PB
NM	NB	NB	PM	NB	Z
PM	NM	PB	PB	Z	PB

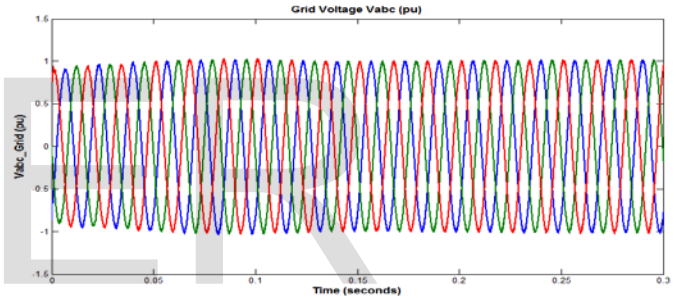

Fig. 15. Gride Voltage in pu

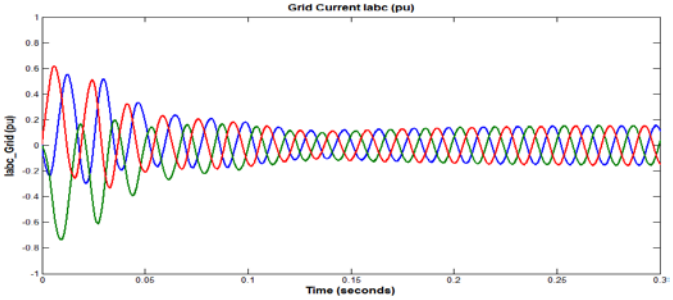

Fig. 16. Gride Current in pu

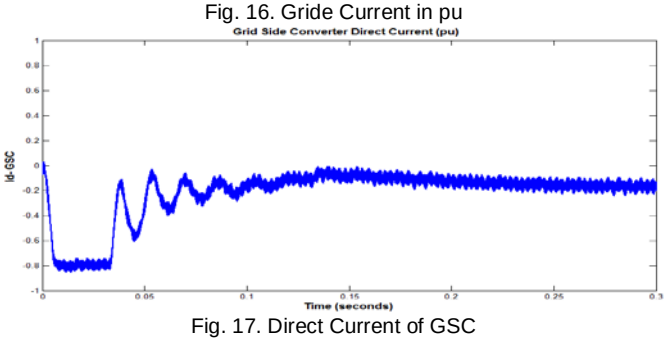

Fig. 17. Direct Current of GSC

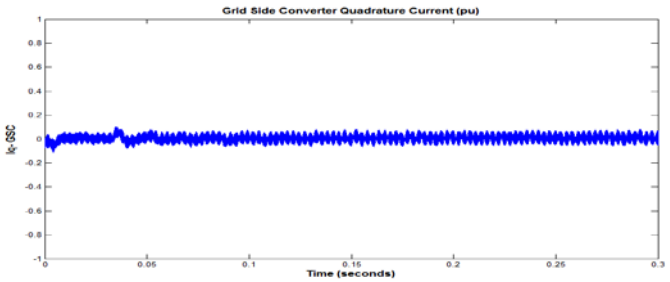

Fig. 18. Quadrature Current of GSC

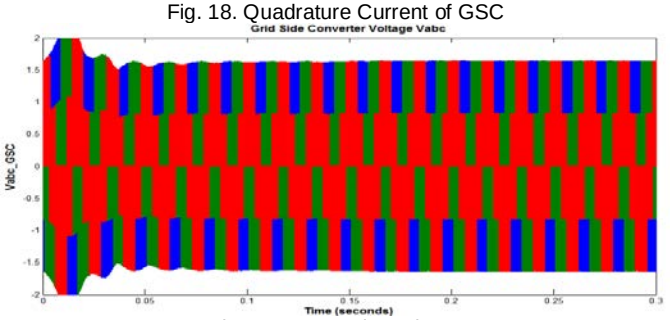

Fig. 19. GSC Voltage in pu

Fig. 19 and Fig. 20 represent GSC three phase voltage and current in per unit. The aim of the DC voltage controller in the outer loop as a cascaded controller that give the suitable set point to the current controller, is to keep the voltage stabilized on its desired value on the DC side during both normal condition, grid faults or due to changes in input power. The inputs for this controller are the desired and measured values for the DC voltage. Error between these two values and its rate of change will be the inputs for the proposed IT2FLC. That controller output will be in turn the reference signal to the d-axis current controller.

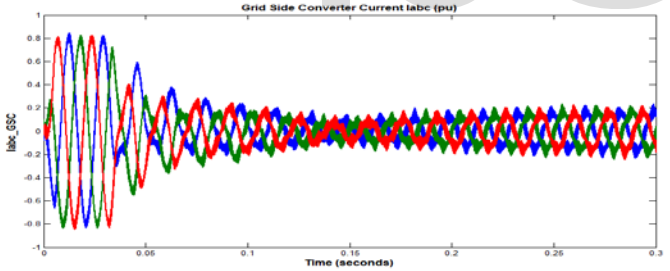

Fig. 20. GSC Current

A PI controller was initially proposed and tested; the transient response of the voltage settled to its final value with 35% peak overshoot and 0.5% steady state error accuracy. While the use of IT2FLC is able to settle the voltage output, after 0.5 seconds, to its final value with 21% peak overshoot and 0.8% steady state accuracy. This result can be shown in Fig. 21.

ACKNOWLEDGMENT

Authors would like to thank Prof. O. Castillo for providing us his own made type-2 fuzzy toolbox [13], his help is much appreciated.

APPENDIX

DFIG parameters:

Nominal power: 1.5 MVA, Rated voltage: 575 Vrms, Frequency: 60 Hz, Magnetizing inductance: 2.9 p.u., Stator resistance: 0.023 p.u., Stator leakage inductance: 0.18 p.u., Rotor resistance: 0.016 p.u., Rotor leakage inductance: 0.16 p.u., Inertia constant: 0.685 s, Friction factor: 0.01 p.u., Number of pairs of poles: 3

DC link characteristics

Nominal DC voltage: 1150 V, Capacitor: 10 mFAuthors would like to thank Prof. O. Castillo for providing us his own made type-2 fuzzy toolbox [13], his help is much appreciated.

REFERENCES

[1] Chandrasena, R. P. S., A. Arulampalam, J. B. Ekanayake, and S. G. Abeyratne. "Grid side converter controller of DFIG for wind power generation." In Industrial and Information Systems, 2007. ICIIS 2007. International Conference on, pp. 141-146. IEEE, 2007.

[2] United Nations Environment Programme, "A Trade Flow Analysis of Selected Environmental Goods," South-South Trade In Renewable Energy, Citation @ UNEP, 2014, South-South trade in renewable energy: A trade flow analysis of selected environmental goods, 104 p.

[3] Xu, Lie, Liangzhong Yao, and Christian Sasse. "Comparison of using SVC and STATCOM for wind farm integration." In Power System Technology, 2006. PowerCon 2006. International Conference on, pp. 1-7. IEEE, 2006.

[4] Hughes, F. Michael, Olimpo Anaya-Lara, Nicholas Jenkins, and Goran Strbac. "Control of DFIG-based wind generation for power network support." Power Systems, IEEE Transactions on 20, no. 4 (2005): 1958-1966.

[5] Kenneth Moore, "Doubly Fed Induction Machine," Director of IEEE Book and Information Services (BIS).

[6] Zhai, Jingjing, and Haoming Liu. "Reactive power control strategy of DFIG wind farms for regulating voltage of power grid." In PES General Meeting | Conference & Exposition, 2014 IEEE, pp. 1-5. IEEE, 2014.

[7] Hani Hagras, and Christian Wagner, " Introduction to Interval Type-2 Fuzzy Logic Controllers - Towards Better Uncertainty Handling in Real World Applications," IEEE SMC - eNewsletter, Issue #27, June 2009.

[8] Ming-Ying Hsiao and Tzuu-Hseng, "Design of Interval Type-2 Fuzzy Logic Controller," IEEE International Conference on Systems, Man, and Cybernetics, October 8-11, 2006, Taipei, Taiwan.

[9] O. M. Salim, M. A. Zohdy, H. Abdel-Aty-Zohdy, H. T. Dorrah and A.M. Kamel, " Type-2 Fuzzy Logic Pitch Controller for Wind Turbine Rotor Blades" , Aerospace and Electronics Conference, Location Dayton OH, Proceedings of the 2011 IEEE National, page 34.

[10] J. M. Mendel, "Uncertain rule-based fuzzy logic systems," Introduction and new directions, Prentice Hall PTR, Upper Saddle River, NJ, 2001.

[11] D.K. Sambariya, R. Gupta, and A. K. Sharma, "Fuzzy Applications to Single Machine Power System Stabilizers," University College of Engineering, Journal of Theoretical and Applied Information Technology, Rajasthan Technical University, Kota, Rajasthan, India-324010, 2005 - 2009.

[12] Jenica Ileana Corcau, and Eleonor Stoenescu, "Fuzzy Logic Controller as a Power System Stabilizer," International Journal of Circuits, Systems and Signal Processing, Volume 1, Issue 3, 2007.

[13] Interval Type-2 Fuzzy Logic Toolbox for use with Matlab, 2005 – 2008, Tijuana Institute of Technology and Baja California Autonomous University.